Science of the Total Environment 711 (2020) 134579

Contents lists available at ScienceDirect

Science of the Total Environment

journal homepage: www.elsevier.com/locate/scitotenv

Trends and drivers of land surface temperature along the urban-rural gradients in the largest urban agglomeration of China

Wenxiao Jia, Shuqing Zhao *

College of Urban and Environmental Sciences, and Key Laboratory for Earth Surface Processes of the Ministry of Education, Peking University, Beijing 100871, China

HIGHLIGHTS

- LST increased along urban-rural gradients.
- Large LST variability existed within the same urban intensity.
- Cities provided ready-made solutions for mitigating urban heat.
- The planning and design of urban landscape were feasible heat mitigation strategies.
- The heat mitigation potential was limited once urban intensity exceeding critical thresholds.

GRAPHICAL ABSTRACT

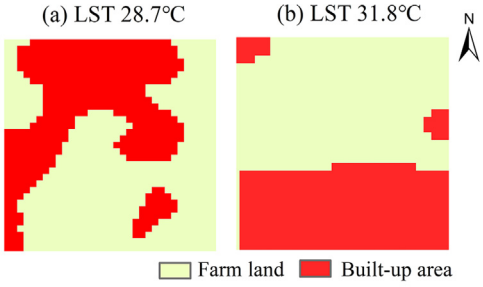

Different landscape structure with the same urban intensity and resultant different land surface temperature (LST)

ARTICLE INFO

Article history:
Received 12 June 2019
Received in revised form 17 September 2019
Accepted 19 September 2019
Available online 20 November 2019

Editor: Dr Deyi Hou

Keywords:
Climate change
Urban-rural gradients
MODIS land surface temperature
Urban agglomeration
Landscape structure

ABSTRACT

Urban heat magnitude and effects may represent harbingers of future climate change and the urban-rural gradients provide a unique natural laboratory for identifying both problems and solutions to climate change mitigation and adaptation. Here, we explored the trends and driving forces of land surface temperature (LST) along the urban-rural gradients of 26 cities in the largest urban agglomeration of China, the Yangtze River Delta Urban Agglomeration, using MODIS LST data combined with urban intensity, background climate, vegetation greenness, landscape structure, albedo, population and gross domestic product (GDP). We found that LST generally increased with increasing urban intensity along the urban-rural gradients while with large diurnal and seasonal variability. Large variability also existed between the maximum and minimum LST within the same urban intensity (e.g., 6.4 °C), suggesting cities themselves provide ready-made solutions (minimum) to resolving heat island problems. However, the range of LST within the same intensity decreased with the urban intensity and narrowed drastically when the intensity reached certain thresholds (e.g., 58–87% varying with season, time of day, and city), implying that the space for climate mitigation is very limited once the urbanization intensity exceeds critical thresholds. The roles of landscape structure (composition and configuration) for greenspace and urban land have become increasingly important in driving the variation of LST with increasing urban intensity from low (20%–30%), middle (45%–55%) to high (70%–80%), clearly indicating that subtle urban landscape designing, such as less aggregated urban configuration and more irregular greenspace shape are effective strategies to mitigate climate change in highly urbanized areas and cities themselves already provide such vivid demonstrations for us to find and learn.

* Correspondence author.
E-mail address: sqzhao@urban.pku.edu.cn (S. Zhao).

https://doi.org/10.1016/j.scitotenv.2019.134579
0048-9697/

1. Introduction

With the rapid urbanization process, natural land surfaces are gradually replaced by impervious surfaces, such as cement, asphalt, and concrete. This change causes notable perturbations to the earth's surface energy balance, resulting in the well-known urban heat island phenomenon, which has been extensively documented and studied in many cities across the world (e.g. Kalnay and Cai, 2003; Peng et al., 2012; Zhou et al., 2014). The magnitude and effects of urban heat island may represent harbingers of future climate change, as already-observed temperature increases within cities exceed the predicted rise in global temperature for the next several decades (Grimm et al., 2008), and further urbanization around the globe has become an irreversible trend. The urban heat island effect also has a profound impact on the lives and health of city dwellers, who account for 55% of the world's population (DESA/UN-WUP, 2018). Since most land surfaces are occupied by impervious surfaces in highly urbanized areas, there is not much space left to reduce urban heat island through increasing vegetation cover in an increasingly urbanized world. Given these circumstances we believe the high priority should be placed on the configuration of greenspace, will it be possible to reduce the influence of urban heat island by changing the interior landscape configuration in an urban system within the same urban green space area? The land parcels with different landscape configuration under the same intensity of urbanization have provided natural laboratory to investigate the possible solutions for urban heat problems. Hence, the analysis and identification of temperature variation and drivers along urban-rural gradient are critically significant for future climate mitigation strategies and scientific urban planning (Arnfield, 2003; Imhoff et al., 2010).

Earlier urban-rural heat research was conducted based on meteorological observations (Fast et al., 2005; Chow and Roth, 2006). Due to the sparsely distributed observation sites, it is difficult to gain a holistic understanding on spatial distribution temperature for such studies. With the rapid development of satellite technology, land surface temperature (LST) derived from the satellite images is widely applied in recent studies (Imhoff et al., 2010; Estoque et al., 2017; Yao et al., 2017, 2018a,b; Zhou et al., 2018). Scholars have demonstrated that LST is closely related to land cover pattern, local background climate, anthropogenic heat sources and increased impervious surfaces and the size of the urban area (Coseo and Larsen, 2014; Debbage and Shepherd, 2015; Lazzarini et al., 2015; Zhao et al., 2014). However, the patterns and driving factors of surface LST remain poorly understood especially for urban agglomerations.

In this paper, using MODIS LST along with urban intensity, background climate, vegetation greenness, population, gross domestic product (GDP), albedo and landscape structure (composition and configuration) of both greenspace and urban land in the year 2015, we investigated the spatial trends and driving forces of LST trends along the urban-rural gradients of 26 cities in the largest urban agglomeration area of China, i.e., the Yangtze River Delta Urban Agglomeration. The specific objectives were (1) to characterize the LST trends along urban-rural gradients in the Urban Agglomeration; (2) to detect the driving factors of LST trends across cities in the Urban Agglomeration; (3) to identify the driving factors of LST within city based on three typical urbanization intensities (low, medium and high).

2. Data and methods

2.1. Study area

The Yangtze River Delta Urban Agglomeration (115°29′–123°44′ E, 27°45′–34°51′ N), located at the junction of the Yangtze River and the East China Sea, covers an area of 215,712 km^2, encompassing 26 cities in total from Jiangsu province, Zhejiang province, Anhui province and Shanghai municipality (Fig. 1). Dominated by marine subtropical monsoon climate, the solar radiation is strong in summer. The mean annual temperature is 16.7 °C, and the mean annual precipitation is 1536 mm (China Meteorological Data Network, 2015). With only 2.2% of the national land areas, the Urban Agglomeration holds 11% of the Chinese population and contributes almost a quarter (22%) of the Chinese national economy (Jiangsu Statistics Bureau, 2015; Shanghai Statistics Bureau, 2015; Zhejiang Statistics Bureau, 2015). It is the most developed, densely populated, and economically vibrant region in China. Due to the strong interference of human activities, the Yangtze River Delta Urban Agglomeration is facing severe environmental problems like urban heat waves, which threaten the health of city dwellers and regional sustainable development (Huang et al., 2010; Tan et al., 2010).

2.2. Remotely sensed LST and urban intensity

Remotely sensed LST products were used to characterize LST along the urban-rural gradients of the Yangtze River Delta Urban Agglomeration. The LST data for the year 2015 were obtained from Aqua MODIS 8-days composite products (version 5) with a spatial resolution of 1 km × 1 km (MYD11A2, version 5 Wan et al., 2015). The LST products were comprised of daytime (13:30) and nighttime (01:30) observations. Summer was defined as the period from June to August, and winter was from December to February, respectively.

The urban intensity in this paper was defined as the percentage of built-up area within the 1 km × 1 km grid, which is equivalent to the spatial resolution of MODIS LST data. The land cover data consisting of six broad categories (farm land, forest, grassland, river and lakes, built-up land and bare soil) for the year 2015, with a spatial resolution 30 m × 30 m were obtained China's National Land Use and Cover Change (CNLUCC) dataset (Xu et al., 2018). It was derived from visual interpretation of Landsat 8 OLI and GF-2 satellite imagery, with reference to the well-established national land use and land cover remote sensing classification system (Liu et al., 2005), unmanned aerial vehicle (UAV) ground survey observation system, and further evaluation by the peer experts (Ning et al., 2018). The overall classification accuracy for the 2015 dataset was more than 93% (Ning et al., 2018). Then the urban intensity was calculated as:

$$UI_i = \frac{UA_i}{TA_i} \times 100\% \quad (1)$$

where UI_i is the urban intensity, UA_i is the area of built-up land, and TA_i is the total area of the ith 1 km × 1 km grid.

We then calculated diurnal and seasonal mean LST for each urban intensity bin from 0 to 100% with an interval of 1% to explore the trends of LST along the urban-rural gradient. This approach ignores physical locations of the pixels, which makes the continuous measure of urban-rural gradient possible. The pixels that were water body, or those with elevations more than 50 m above the highest elevation of urban core (where urban intensity was above 50%), were excluded to avoid the effect of water body or elevation's effect on LST (Fig. 2; Zhou et al., 2015, 2016, 2018). Also, LST range at each urban intensity bin from 0% to 100% was calculated. Piecewise regression was used to identify the thresholds of LST variation along urban intensity gradient.

2.3. Driving forces analysis for both inter-cities and intra-cities

The potential driving forces of LST in this study included background climate, vegetation greenness, landscape structure

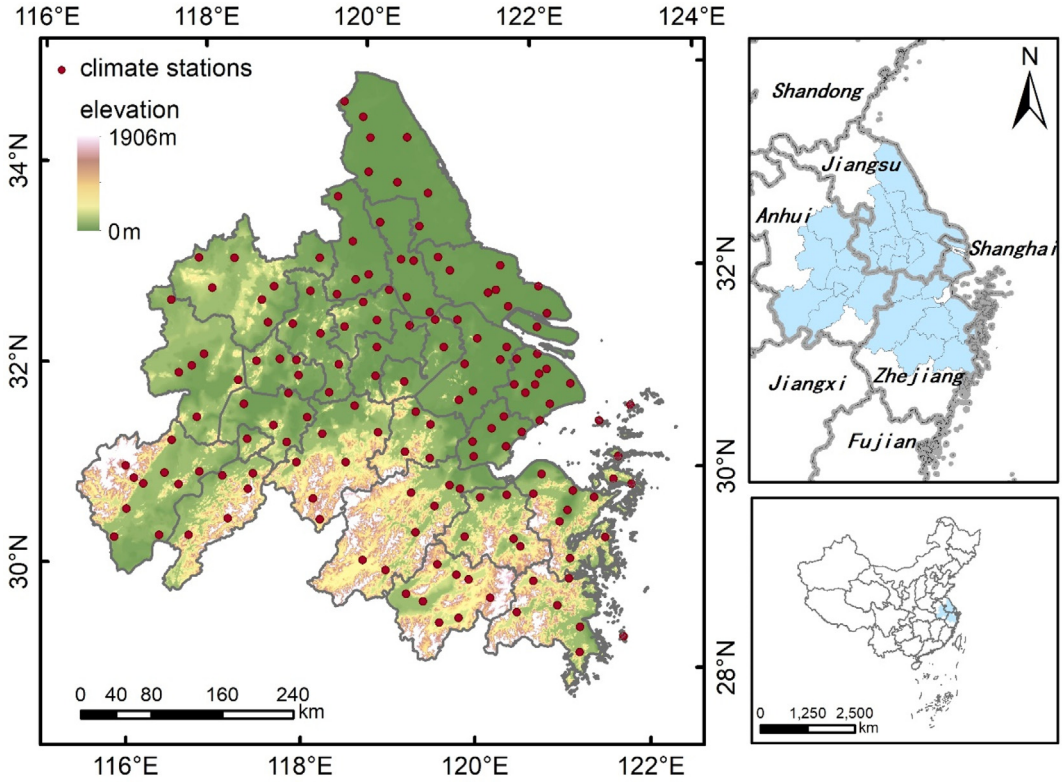

Fig. 1. Location of the study area, with background map showing the climate stations and elevation.

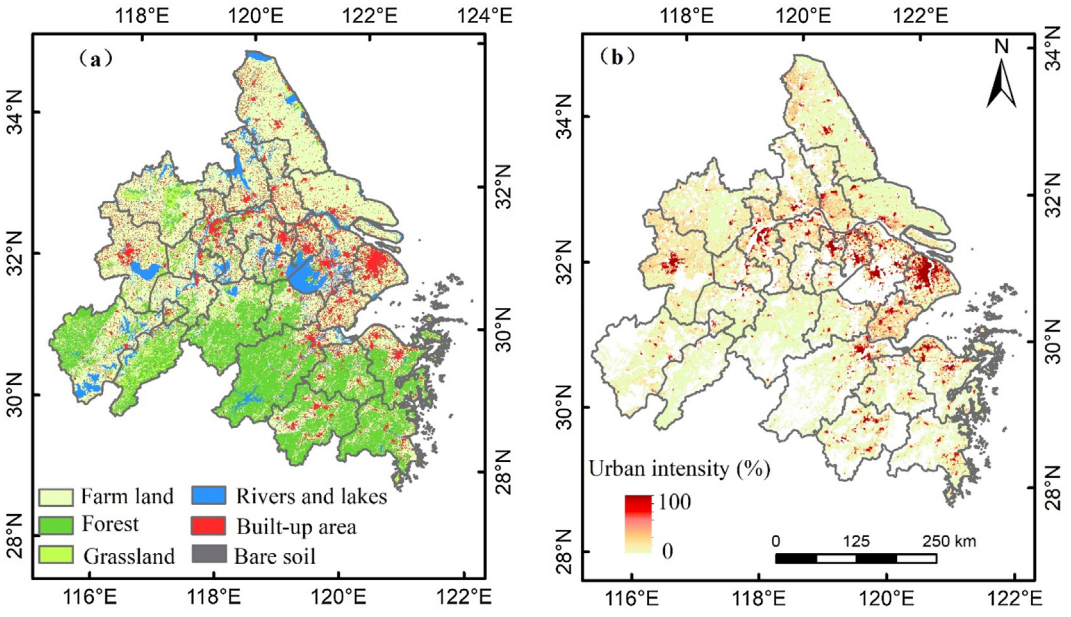

Fig. 2. (a) The land cover map in 2015 derived from China's National Land Use and Cover Change (CNLUCC) dataset (Xu et al., 2018); (b) urban intensity (%) calculated as the percentage of built-up area within the 1 km × 1 km MODIS LST pixel.

(composition and configuration) of both greenspace and urban land, population, Gross Domestic Product (GDP) and albedo for the corresponding year of 2015. The climate observations were extracted from the daily data set produced by China Meteorological Administration. There were 154 weather stations located in the Yangtze River Delta Urban Agglomeration (Fig. 1). The climate data included mean air temperature, precipitation, air pressure, evaporation, wind speed and photosynthetically active radiation (PAR, calculated from sunshine hours and global solar radiation according to Zhu et al. 2010). These climate data were averaged for each station in summer (June, July and August) and winter (December, January and February), and were then interpolated to 1 km × 1 km grid via Anusplin software (Hutchinson, 1995) based on thin plate smoothing spline method taking latitude, longitude and elevation covariates into account. Vegetation greenness characterized by greenspace intensity and vegetation index were used.

Greenspace intensity within each 1 km × 1 km LST grid was calculated as the percentage of sum of forest, farm land and grassland based on the 30 m × 30 m land cover dataset (the same approach as urban intensity). MODIS Enhanced Vegetation Index (EVI) data with a spatial resolution of 250 m × 250 m (MOD13Q1) from the corresponding seasons were collected and averaged within 1 km × 1 km LST grids. Three landscape metrics: mean patch size ($AREA_{MN}$), mean shape index ($SHAPE_{MN}$), and aggregation index (AI), were adopted to reflect the landscape composition and configuration of green spaces and built-up land. $AREA_{MN}$ is the average size of the patches. $SHAPE_{MN}$ describes the shape complexity, and the value increases without limit as patch shape becomes irregular. AI indicates the degree of aggregation. It increases as the focal patch is increasingly aggregated and maximizes when the patch is maximally aggregated into a single, compact patch. They were calculated for each 1 km × 1 km grid using Fragstats 3.3 with 8 cell neighborhood (McGarigal et al., 2002). The population and GDP data for each 1 km × 1 km LST grid were collected from the Resources and Environmental Science Data Center of Chinese Academy of Sciences (http://www.resdc.cn; Xu, 2017a,b). The white-sky albedo (WSA) data from MODIS Bidirectional Reflectance Distribution Function (BRDF) albedo product (MCD43A3) were collected. The WSA were averaged in summer (June, July and August) and winter (December, January and February) within each 1 km × 1 km LST grid.

For inter-cities, we analyzed the driving factors of the LST–urban intensity slope. We used multiple linear regression to extract the driving factors for LST trends along urban-rural gradient in the Urban Agglomeration. Determination coefficient (R^2) was used to analyze the explanation of the selected variables to the variations of LST trend among the Urban Agglomeration in the multiple linear fitting models.

For intra-cities, we analyzed the driving forces of LST variation within each of three typical urban intensity intervals (20%–30%, 45%–55% and 70%–80%, indicating low, medium and high intervals) for each city. We used a relative importance analysis approach to quantify the relative contributions of potential drivers in R "relaimpo" package, which is based on variance decomposition for multiple linear regression models (Grömping, 2006). The relaimpo package has been widely used for separating the relative roles of various factors in ecological studies in recent years (Belmaker and Jetz, 2015; Huang et al., 2018). It aims to explore the contribution of driving forces of LST under different urban intensity intervals in different cities for further effective mitigation and adaption strategies intra-cities.

3. Results

3.1. Trends of LST with rising urban intensity

The LST generally increased with increasing urban intensity but varied with season and daytime/nighttime. In summer, for all cities, the daytime LST increased evidently and rapidly with rising urban intensity. Large variability of LST (the difference between maximum and minimum) within the same urban intensity existed as well (Fig. 3). The LST changes along with urban intensity from 0% to 100% for summer night, winter day and winter night were provided in Figs. S1–S3. The LST–urban intensity trends showed large seasonal and diurnal difference (Fig. 4). On average, the LST–urban intensity trends in summer day were 5.1 ± 1.2 °C (per 100% urban intensity, hereafter). In winter, 20 out of 26 cities exhibited significant increases in daytime ($p < 0.05$), while one city (Yancheng) showed cold island effect with negative LST–urban intensity linear coefficient. The average trends in winter daytime were 0.9 ± 0.8 °C. Xuancheng and Hefei exhibited the steepest slope of summer daytime LST–urban intensity with 7.1 °C and 7.0 °C, while Yancheng was with lowest slope, i.e., 2.7 °C. The LST–urban intensity linear coefficient in winter day ranged from −0.9 °C (Yancheng) to 2.2 °C (Xuancheng and Taizhou2). The mean intercept in summer and winter daytime was 31.5 ± 1.3 °C, 12.6 ± 1.0 °C respectively, which indicated the seasonal difference of rural climate condition in the Urban Agglomeration. The intercept in summer day is largest in Shanghai (33.5 °C).

For nighttime trends, the average summer trend was 0.9 ± 0.6 °C, higher than that in winter (0.2 ± 0.5 °C). 22 out of 26 cities exhibited significant upward LST–urban intensity trends in summer ($p < 0.05$). Only 14 of 26 cities were with significant increasing nighttime LST along rising urban intensity in winter, whereas eight cities indicated insignificant linear LST–urban intensity relationship and four cities were with cold island effects. Relative to the daytime, the nighttime LST showed a mild rising pattern with urban intensity. The trend ranged from −0.1 °C (Changzhou) to 1.9 °C (Shaoxing and Jinhua) in summer, −1.0 °C (Zhoushan) to 1.4 °C (Chuzhou) in winter. The mean nighttime LST–urban intensity linear intercept in summer was 21.5 ± 0.7 °C, in winter was 1. 0 ± 1.5 °C. Correlation analysis showed that the trends in summer and winter daytime for 26 cities in the Urban Agglomeration were significantly correlated (r = 0. 51, p < 0.01), whereas nighttime trends in summer and winter were not significantly correlated.

3.2. The drivers of LST–urban intensity trend for the Urban Agglomeration

The multiple linear regression results of LST–urban intensity trend were showed in Table 1. LST–urban intensity trend was significantly correlated with evaporation (r = 0.82, $p < 0.001$) in summer day, and evaporation was the primary driver of daytime LST–urban intensity trend over the Urban Agglomeration (R^2 = 0.55). In summer nighttime, evaporation and vegetation $SHAPE_{MN}$ were important drivers for LST–urban intensity trend variation among 26 cities (R^2 = 0.61). The LST trends had significant positive correlations with evaporation (r = 0.62, $p < 0.01$) and vegetation $SHAPE_{MN}$ (r = 0.61, $p < 0.01$). In winter, the daytime LST trend variation was contributed most from air temperature, with R^2 = 0.75. The LST changing rates along urban intensity was significantly correlated with air temperature (r = 0.87, $p < 0.001$). In winter nighttime, LST changing rate was most contributed by urban $AREA_{MN}$ (R^2 = 0.30). It presented significant positive correlations with urban $AREA_{MN}$ (r = 0.55, $p < 0.01$), GDP (r = 0.53, $p < 0.05$), urban AI (r = 0.53, $p < 0.05$), urban $SHAPE_{MN}$ (r = 0.50, $p < 0.05$).

3.3. The drivers of LST variation in typical urban intensity gradients

The LST differences between hottest pixels and coldest pixels in the same bin averaged to be ca 6.4 °C in summer day, higher than 3.2 °C in summer night, 4.6 °C in winter day and 2.7 °C in winter night, which indicated the chance for urban heat mitigation strategies. The LST range between maximum and minimum deceased with the increase of urban intensity. We obtained a mean threshold value of 86.7% urban intensity in summer day, which meant that generally, when urban intensity was less than 86.7%, the LST fluctuated greatly among the same urban intensity. And when urban intensity was larger than 86.7%, the LST range sharply reduced to minimum. And the winter daytime threshold value averaged at 63.0% urban intensity among 26 cities. The nighttime threshold value for summer and winter averaged at 58.3%, 65.3% urban intensity respectively. Fig. 5 shows the demonstrations of several cities to identify the thresholds of relationship between the LST range and urban intensity.

Since maximum-minimum LST difference within each urban intensity bin for most cities is large, especially in summer day,

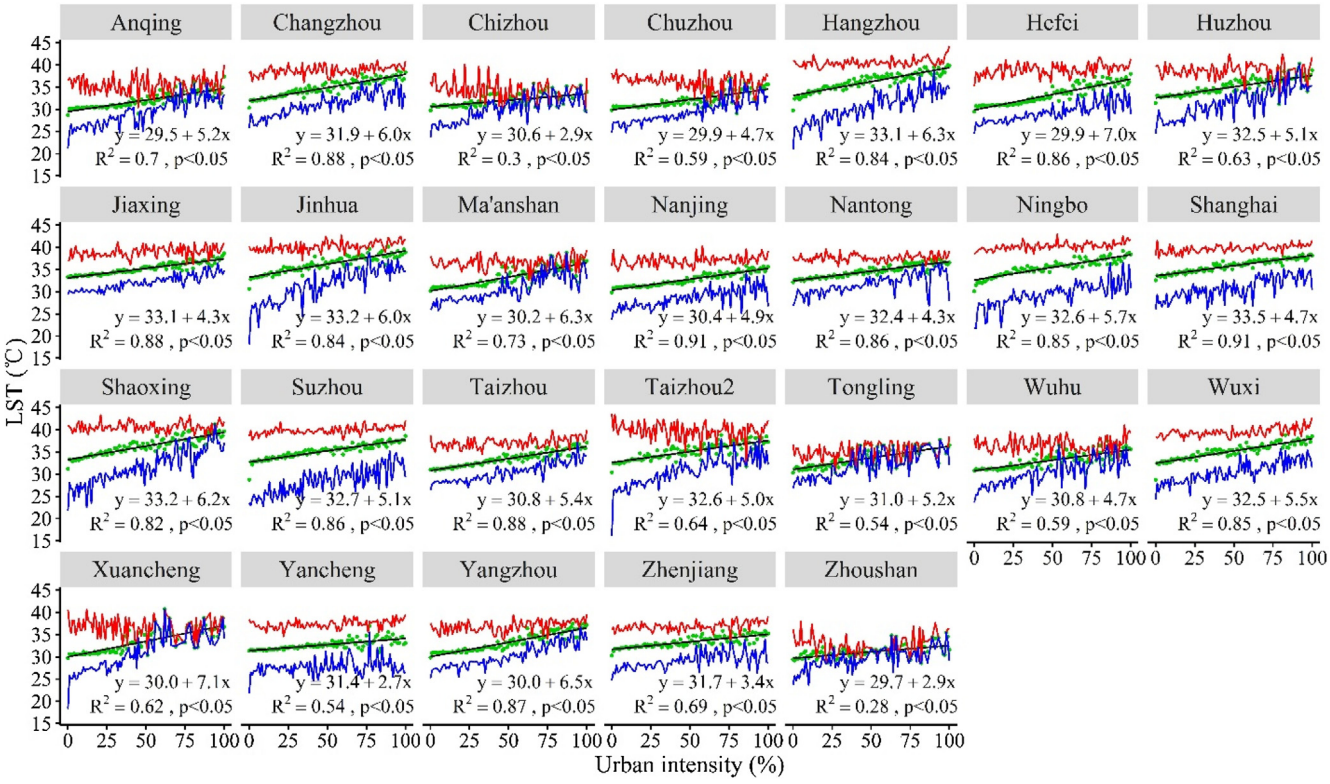

Fig. 3. The maximum (red line), mean (green dots) and minimum (blue line) of summer daytime LST along urban intensity gradient (0–100%) in 26 cities of the Urban Agglomeration. (For interpretation of the references to colour in this figure legend, the reader is referred to the web version of this article.)

we attempted to look into the detailed drivers of LST variation within the same urban intensity of the same city. Three typical urbanization gradients: low (L, 20%~30%), middle (M, 45%~55%) and high (H, 70%~80%) were chosen to further analyze the driving forces of LST variation in summer day (Fig. 6). Small cities (i.e., Ma'anshan, Chizhou, Chuzhou, Wuhu, Zhoushan, etc.) were excluded for this part because the pixel samples within certain urban intensity gradients in these cities were very scarce. For example, there are only 15 pixels in urban intensity bin of 70~80% for Zhoushan. The results showed that EVI was the dominant drivers for LST variation in summer day for the cities. The contribution of climate drivers (temperate, precipitation, evaporation) to LST variation in high urban intensity bins was the lowest among three typical urban intensity gradients. In contrast, the landscape structure (composition and configuration) of both greenspace and urban land played an increasing role with increasing unban intensity, although its contribution was still small relative to EVI. That is, the addition of green space to urban landscape is the vital strategy for urban heat mitigation, however, given the circumstance of same or similar building area quantity, especially for the high urban intensity end with insufficient land use for greenspaces, more attention should be paid to the landscape structure designing in the mitigation of urban heat. Specifically, in low urban gradient, most cities exhibited insignificant correlation with landscape structure except Suzhou city. In Suzhou, urban $AREA_{MN}$ was significantly negative correlated with LST ($r = -0.15$, $p < 0.05$). Vegetation $AREA_{MN}$ is significantly positive correlated with LST ($r = 0.14$, $p < 0.05$), while vegetation $SHAPE_{MN}$ is significantly negative with LST ($r = -0.14$, $p < 0.05$). In medium urban intensity gradient, several cities exhibited significant correlation with landscape structure. For example, in Changzhou there was significant negative correlation between urban AI and LST ($r = -0.30$, $p < 0.05$), and vegetation $AREA_{MN}$, vegetation AI and vegetation $SHAPE_{MN}$ were negatively correlated with LST variation ($r = -0.33$, -0.26, -0.19, respectively) in Nanjing. In high urban gradient, the landscape structure played important roles in LST variation for many cities. For example, LST variation in Jinhua was negatively associated with vegetation $AREA_{MN}$ ($r = -0.35$) and vegetation $SHAPE_{MN}$ ($r = -0.31$), and positively correlated with urban $SHAPE_{MN}$ ($r = 0.41$, $p < 0.05$). In both Nantong and Ningbo, urban AI significantly and positively correlated with LST variation ($r = 0.55$, $p < 0.05$). The vegetation $AREA_{MN}$ ($r = -0.43$) and vegetation $SHAPE_{MN}$ ($r = -0.45$) had an important effect on LST variation in Shaoxing.

4. Discussion

4.1. Trends of LST with rising urban intensity in the Urban Agglomeration

LST significantly increased with rising urban intensity during the day and night both in summer and winter for most cities in the Yangtze River Delta Urban Agglomeration. This finding is consistent with former research on urban thermal environment in the United States (Imhoff et al., 2010) and Chinese 32 major cities (Zhou et al., 2014, 2016). Our results were quite close to Zhou et al. (2018). They found the summer daytime trend was 4.7 ± 1.2 °C (comparable to our estimate of 5.1 ± 1.2 °C), the winter daytime trend was 0.5 ± 0.8 °C (0.9 ± 0.8 °C), via the method defined the temperature difference as urban pixel relative to forest base condition, which corresponded to the urban-rural two ends along the entire urban to rural spectrum. The slight difference might be related to the data processing method and study period. However, our estimate of LST trend along the urban-rural gradient in summer daytime (5.1 ± 1.2 °C) was much higher than the finding

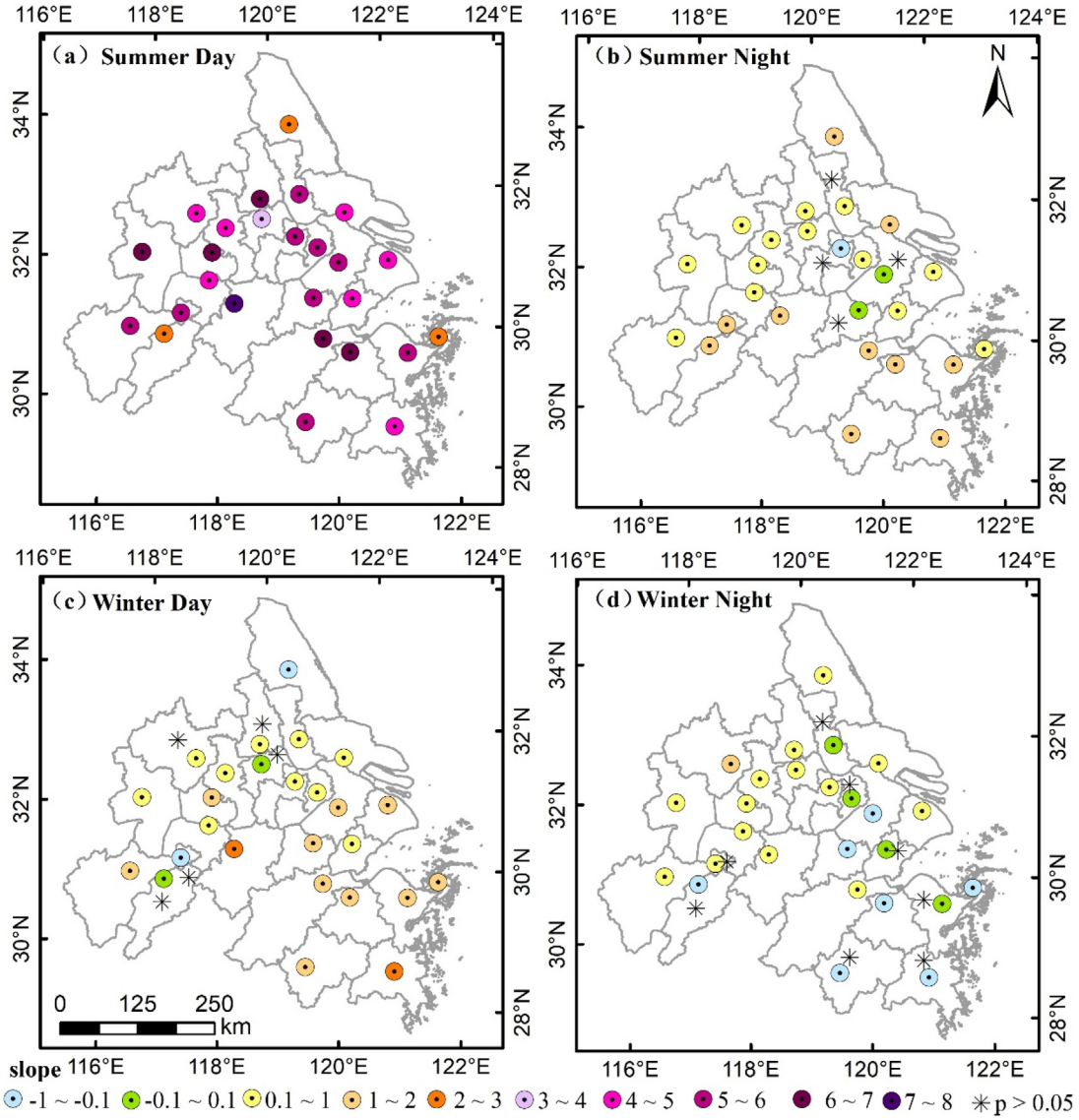

Fig. 4. Spatial patterns of LST trend along urban intensity from 0% to 100% in 26 cities of the Yangtze River Delta Urban Agglomeration. Cities with star sign were with insignificant linear trends ($p > 0.05$), otherwise significant ($p < 0.05$).

Table 1
Multiple linear regression results of LST-urban intensity trend.

LST–urban intensity slope	Multiple linear regression	R^2
Daytime in summer	$slope = -20.66 + 0.25 \times EVP$	0.55***
Nighttime in summer	$slope = -38.64 + 0.01 \times EVP + 0.38 \times (vegSHAPE_{MN})$	0.61***
Daytime in winter	$slope = -3.95 + 0.05 \times T$	0.75***
Nighttime in winter	$slope = -0.47 + 0.02 \times (urbanAREA_{MN})$	0.30**

Significant at the 0.01 level, * significant at the 0.001 level. EVP: evaporation; T: air temperature; veg SHAPEMN: vegetation SHAPEMN.

from a previous study on the Urban Agglomeration that found the temperature difference between urban and suburban was 1.1 °C during summer daytime (Du et al., 2016a,b). This discrepancy was related to the fact that urban/suburban difference tends to underestimate urban heat island intensity because suburbanization generally occurs, particularly in highly developed regions. Compared to traditional urban heat island effect studies based on two ends of temperature difference (Du et al., 2016a,b; Yao et al., 2017; Zhou et al., 2014), the urban-rural gradient approach provides a comprehensive understanding of urban thermal environment along the entire spectrum from urban to rural (Li et al., 2018).

There was significant spatial heterogeneity in trends of LST along rising urban intensity among the Urban Agglomeration region. The different patterns during the day and night in both seasons might be largely due to the different identified dominant drivers. The variation of LST–urban intensity trends among cities during daytime in summer was largely contributed to regional evaporation variability. Cities of the Urban Agglomeration were with hot and humid climate. The higher soil water content usually presents in rural area than densely developed area covered by impervious surfaces (Zhou et al., 2016), resulting in higher evaporative cooling and lower LST in the rural area. Hence, the cities with higher mean evaporation tended to exhibit a steeper relationship between daytime LST and urban intensity in summer. Evaporation and vegetation $SHAPE_{MN}$ were significant drivers for nighttime LST–urban intensity trend variation among 26 cities in summer.

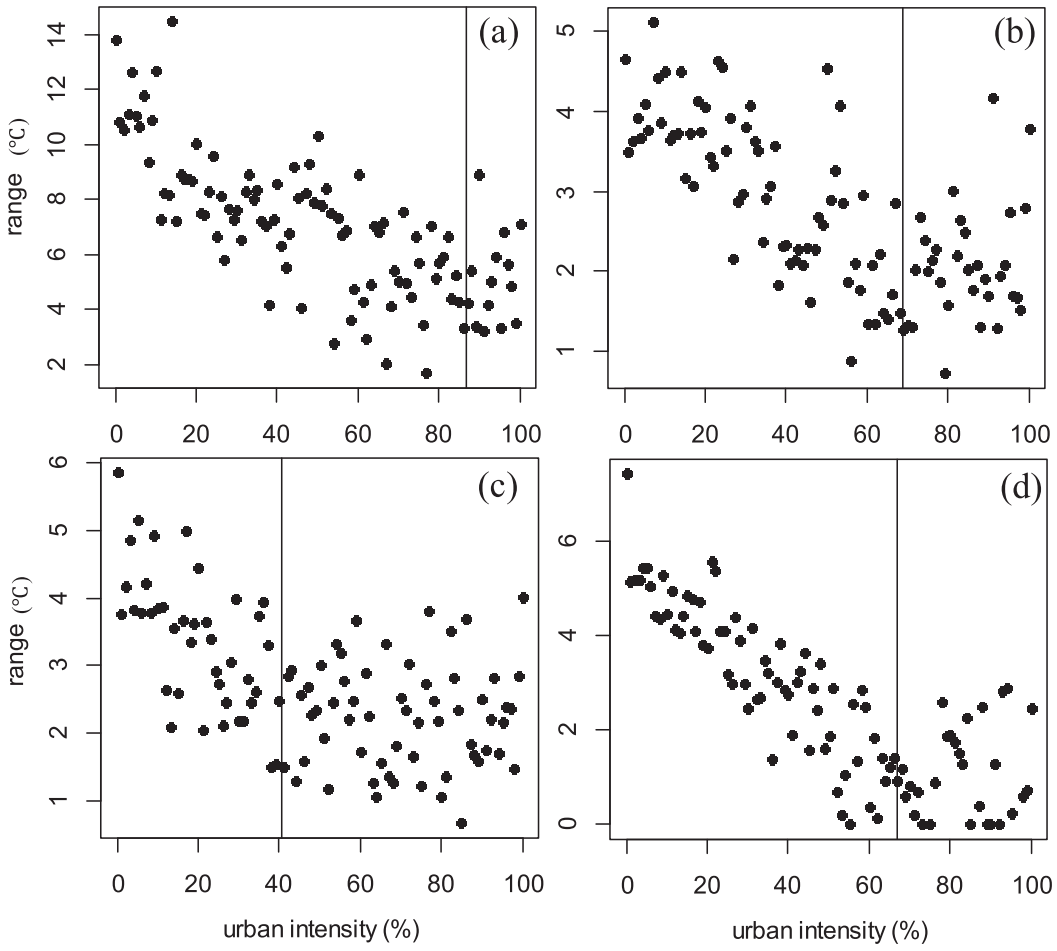

Fig. 5. Demonstrations for the thresholds of relationship between the LST range and urban intensity in (a) summer day, Jinhua city (b) summer night, Wuxi city (c) winter day, Wuxi city (d) winter night, Anqing city.

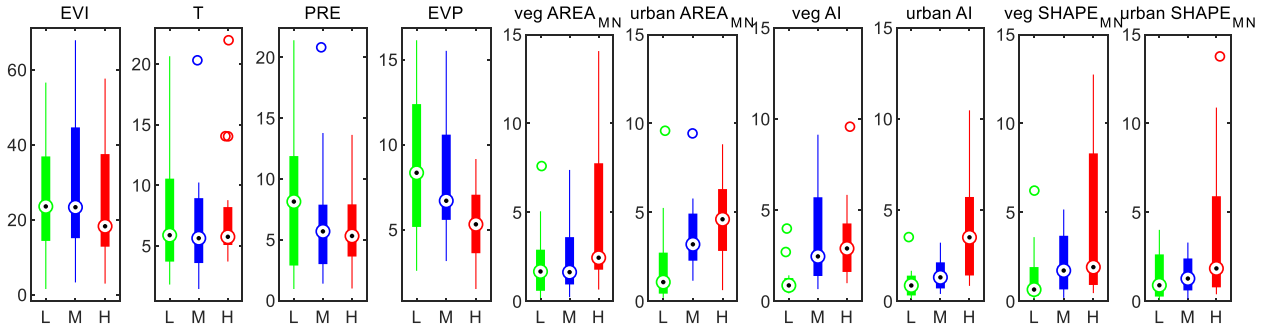

Fig. 6. Relative contribution of different drivers to summer daytime LST variation (relative importance, %) in low (L), medium (M) and high (H) urban intensity intervals. The medians, the 25th and 75th percentiles were visualized in the bars and the outliers were represented as hollow points.

The vegetation $SHAPE_{MN}$ equals 1 when the green patch is square and increases without limit as green patch shape becomes more irregular. The increases of green patch edges along with increasing shape complexity enhance the energy flow between green patches and surrounding environment, which could also lower the rural area LST. The negative relationship between LST and green patches shape complexity was supported by other studies (Zhou et al., 2011; Maimaitiyiming et al., 2014). And the lower LST in rural area could increase the LST trends (Yao et al., 2019). Temperature was the dominant contributor in winter daytime LST trend. Cities with higher temperature in winter day were with larger LST trend. The LST–urban intensity trends in winter day were negatively correlated with average wind speed. The low temperatures and heavy winds accelerate temperature exchange between urban and surrounding areas during winter, resulting in a decreased LST–urban intensity slope in the Urban Agglomeration. The winter nighttime variation was contributed most from urban $AREA_{MN}$. Cities with larger urban $AREA_{MN}$ possess larger amount of impervious surfaces, larger population, and consume larger amount of energy, which can expand the LST gap between rural and urban area (Du et al., 2016a,b). We also find that in this urban agglomeration, the urban size (reflected by GDP and urban $AREA_{MN}$) could contribute positively to LST–urban intensity trends especially in winter night. This denotes that in winter night, the LST–urban

intensity trends were mainly contributed by anthropogenic heat emissions. The nighttime LST–urban intensity trends were the consequence of more surface heat storage in highly urbanized area due to anthropogenic heat emissions from industrial, traffic and air conditioner within domestic buildings. Also, the trend of the closely connected metropolitan areas (i.e., Shanghai, Suzhou and Wuxi) might be underestimated due to the urban agglomeration effect (Zhou et al., 2018). The pixels of the rural areas decrease with accelerating urban land expansion and the rural area might be affected by the transcended urban heat with the disappearing distances among urban areas.

4.2. Implications for urban design and planning for future climate change mitigation

Further urbanization around the globe has become an irreversible trend. Also, the observed temperature increases within cities already exceed the predicted rise in global temperature for the next several decades (Grimm et al., 2008). The urban heat environment provides a vivid natural lab along a rural-urban gradient for future global temperature rise prediction and mitigation. Large LST variation within the same urban intensity (e.g., 6.4 °C), gave us some hints for further urban design and heat mitigation strategies. Cities themselves provide ready-made solutions (minimum LST within the same rural-urban gradient) to resolving heat island problems. However, the range of LST within the same urban intensity decreased with the rural-urban gradient, indicating that the marginal heat mitigation probability is decreasing with increasing urban intensity along the urban-rural gradient for most cities in the Urban Agglomeration. Also, the LST range narrowed drastically when urban intensity reached certain thresholds (e.g., 58–87% varying with season, time of day and city), implying that the space for climate mitigation is very limited once the urbanization intensity exceeds critical thresholds.

None of previous studies have detected the threshold value of urban intensity for the variation of LST range along the rural-urban gradient. The urban heat island is severest in summer day, which is consistent with former studies (Zhou et al., 2018, 2014). The LST range threshold urban intensity in summer day is 87%, indicating there will be no possibility for urban heat mitigation measures when the urban intensity beyond this threshold. We analyzed the drivers of summer daytime LST variation within three typical urban intensity bins: low (20%–30%), middle (45%–55%) to high (70%–80%). The roles of landscape structure (composition and configuration) for greenspace and urban land have become increasingly important in driving the variation of LST with increasing urban intensity from low (20%–30%), middle (45%–55%) to high (70%–80%), clearly indicating that subtle urban landscape designing, such as less aggregated urban configuration and more irregular greenspace shape are effective strategies to mitigate climate change in highly urbanized areas. Moreover, many urban residents dwell in highly urbanized areas that might suffer from strong urban heat island and heat wave effects, indicating the great significance of urban landscape designing.

4.3. Limitations and suggested future research

This study illustrated LST variation along the urban intensity gradient, while it omitted the physical distance to urban core, another critical indicator affecting urban thermal environment. The LST is not only determined by the corresponding pixel, but also affected by the adjacent pixels. A new indicator coupled both urban intensity and physical distance is needed to fully illustrate the urban heat condition along the urban-rural gradient. Also, Zhou et al. (2015) has indicated that the footprint of urban heat island effect was 2.3 and 3.9 times of urban size for the day and night, respectively. In urban agglomerations, with the inter-cities border gradually disappearing and urban core area densely developed, the footprint of urban heat island effect is enlarging and might affect adjacent cities. The heat interactions among cities in highly cooperated urban agglomerations might bring us new insights in further studies. Furthermore, more complicated factors like building height (Allegrini and Carmeliet, 2017; Perini and Magliocco, 2014), vegetation canopy (Howe et al., 2017), and haze pollution (Cao et al., 2016) could also affect the urban surface energy exchange. Also, this paper omitted the water body factor, which played a significant role in mitigation urban heat island effects (Du et al., 2016a,b). We focus on identifying the possible heat mitigating solutions from already-existed landscape composition and configuration of urban land and greenspace, which are more feasible to adopt in urban planning and design than water bodies. In addition, the spatial interpolation of meteorological data might bring some uncertainty to our driving forces analysis. Complementary and direct observations are needed to understand the underlying mechanisms of urban thermal environment for the better understanding and successful mitigation and adaptation strategies.

Contemporary urban heat environment and mitigation strategies might provide valuable information for future global warming condition in low urbanization in the next several decades as climate change and urbanization processes continue. Also, the impervious surface replacement and energy consumption has intensified global warming, which in turn has exacerbated the urban land surface heat environment and processes (Arnfield, 2003; Liu et al., 2017). Thus, successful urban-scale heat mitigation strategies and practices can bring co-benefits for large-scale climate change mitigation and adaptation (Stocker et al., 2013). Moreover, using cities as natural laboratories to develop and test hypotheses about global warming and its impacts remains untested due to the large disparities between urban ecosystems and natural ecosystems (Grimm et al., 2008). Future studies need complementary urban and long-term observations (Youngsteadt et al, 2015).

Declaration of Competing Interest

The authors declare that there is no conflict of interest regarding the publication of this article.

Acknowledgements

This study was supported by the National Natural Science Foundation of China Grants 41771093 and 41571079. We acknowledge the data support of "Geographic Data Sharing Infrastructure, College of Urban and Environmental Science, Peking University (http://geodata.pku.edu.cn)".

Appendix A. Supplementary data

Supplementary data to this article can be found online at https://doi.org/10.1016/j.scitotenv.2019.134579.

References

Allegrini, J., Carmeliet, J., 2017. Coupled CFD and building energy simulations for studying the impacts of building height topology and buoyancy on local urban microclimates. Urban Clim. 21, 278–305. https://doi.org/10.1016/j.uclim.2017.07.005.

Arnfield, A.J., 2003. Two decades of urban climate research: a review of turbulence, exchanges of energy and water, and the urban heat island. Int. J. Climatol. https://doi.org/10.1002/joc.859.

Belmaker, J., Jetz, W., 2015. Relative roles of ecological and energetic constraints, diversification rates and region history on global species richness gradients. Ecol. Lett. https://doi.org/10.1111/ele.12438.

Cao, C., Lee, X., Liu, S., Schultz, N., Xiao, W., Zhang, M., Zhao, L., 2016. Urban heat islands in China enhanced by haze pollution. Nat. Commun. 7. https://doi.org/10.1038/ncomms12509.

Chow, W.T.L., Roth, M., 2006. Temporal dynamics of the urban heat island of Singapore. Int. J. Climatol. https://doi.org/10.1002/joc.1364.

Coseo, P., Larsen, L., 2014. How factors of land use/land cover, building configuration, and adjacent heat sources and sinks explain Urban Heat Islands in Chicago. Landsc. Urban Plan. https://doi.org/10.1016/j.landurbplan.2014.02.019.

Debbage, N., Shepherd, J.M., 2015. The urban heat island effect and city contiguity. Comput. Environ. Urban Syst. https://doi.org/10.1016/j.compenvurbsys.2015.z08.002.

DESA/UN-WUP, 2018. World Urbanization Prospects: The 2018 Revision. Dep. Econ. Soc. Aff.

Du, H., Wang, D., Wang, Y., Zhao, X., Qin, F., Jiang, H., Cai, Y., 2016a. Influences of land cover types, meteorological conditions, anthropogenic heat and urban area on surface urban heat island in the Yangtze River Delta Urban Agglomeration. Sci. Total Environ. 571, 461–470. https://doi.org/10.1016/j.scitotenv.2016.07.012.

Du, H., Song, X., Jiang, H., Kan, Z., Wang, Z., Cai, Y., 2016b. Research on the cooling island effects of water body: a case study of Shanghai, China. Ecol. Indic. https://doi.org/10.1016/j.ecolind.2016.02.040.

Estoque, R.C., Murayama, Y., Myint, S.W., 2017. Effects of landscape composition and pattern on land surface temperature: an urban heat island study in the megacities of Southeast Asia. Sci. Total Environ. 577, 349–359. https://doi.org/10.1016/j.scitotenv.2016.10.195.

Fast, J.D., Torcolini, J.C., Redman, R., 2005. Pseudovertical temperature profiles and the urban heat island measured by a temperature datalogger network in Phoenix, Arizona. J. Appl. Meteorol. https://doi.org/10.1175/jam-2176.1.

Grimm, N.B., Faeth, S.H., Golubiewski, N.E., Redman, C.L., Wu, J., Bai, X., Briggs, J.M., 2008. Global change and the ecology of cities. Science (80-). https://doi.org/10.1126/science.1150195.

Grömping, U., 2006. Relative importance for linear regression in R: the package relaimpo. J. Stat. Softw.

Howe, D.A., Hathaway, J.M., Ellis, K.N., Mason, L.R., 2017. Spatial and temporal variability of air temperature across urban neighborhoods with varying amounts of tree canopy. Urban For. Urban Green. 27, 109–116. https://doi.org/10.1016/j.ufug.2017.07.001.

Huang, K., Xia, J., Wang, Y., Ahlström, A., Chen, J., Cook, R.B., Cui, E., Fang, Y., Fisher, J.B., Huntzinger, D.N., Li, Z., Michalak, A.M., Qiao, Y., Schaefer, K., Schwalm, C., Wang, J., Wei, Y., Xu, X., Yan, L., Bian, C., Luo, Y., 2018. Enhanced peak growth of global vegetation and its key mechanisms. Nat. Ecol. Evol. https://doi.org/10.1038/s41559-018-0714-0.

Huang, W., Kan, H., Kovats, S., 2010. The impact of the 2003 heat wave on mortality in Shanghai. China. Sci. Total Environ. 408, 2418–2420. https://doi.org/10.1016/j.scitotenv.2010.02.009.

Hutchinson, M.F., 1995. Interpolating mean rainfall using thin plate smoothing splines. Int. J. Geogr. Inf. Syst. https://doi.org/10.1080/02693799508902045.

Imhoff, M.L., Zhang, P., Wolfe, R.E., Bounoua, L., 2010. Remote sensing of the urban heat island effect across biomes in the continental USA. Remote Sens. Environ. https://doi.org/10.1016/j.rse.2009.10.008.

Jiangsu Statistics Bureau, 2015. Jiangsu Statistical Yearbook 2014. China Statistics Press, Beijing.

Kalnay, E., Cai, M., 2003. Impact of urbanization and land-use change on climate. Nature 423. https://doi.org/10.1038/nature01675.

Lazzarini, M., Molini, A., Marpu, P.R., Ouarda, T.B.M.J., Ghedira, H., 2015. Urban climate modifications in hot desert cities: THE role of land cover, local climate, and seasonality. Geophys. Res. Lett. 42, 9980–9989. https://doi.org/10.1002/2015GL066534.

Li, H., Zhou, Y., Li, X., Meng, L., Wang, X., Wu, S., Sodoudi, S., 2018. A new method to quantify surface urban heat island intensity. Sci. Total Environ. 624, 262–272. https://doi.org/10.1016/j.scitotenv.2017.11.360.

Liu, J., Tian, H., Liu, M., Zhuang, D., Melillo, J.M., Zhang, Z., 2005. China's changing landscape during the 1990s: Large-scale land transformations estimated with satellite data. Geophys. Res. Lett. 32 (2).

Liu, S., Bond-Lamberty, B., Boysen, L.R., Ford, J.D., Fox, A., Gallo, K., Hatfield, J., Henebry, G.M., Huntington, T.G., Liu, Z., Lovelan, T.R., Norby, R.J., Soh, T., Steiner, A.L., Yuan, W., Zhang, Z., Zhao, S., 2017. Grand challenges in understanding the interplay of climate and land changes. Earth Interact. https://doi.org/10.1175/EI-D-16-0012.1.

Maimaitiyiming, M., Ghulam, A., Tiyip, T., Pla, F., Latorre-Carmona, P., Halik, U., Sawut, M., Caetano, M., 2014. Effects of green space spatial pattern on land surface temperature: implications for sustainable urban planning and climate change adaptation. Isprs J. Photogramm. Remote Sens. 89, 59–66. https://doi.org/10.1016/j.isprsjprs.2013.12.010.

McGarigal, K., Cushman, S.A., Neel, M.C., Ene, E., 2002. FRAGSTATS: Spatial Pattern Analysis Program for Categorical Maps. Analysis. https://doi.org/Cited By (since 1996) 586\rExport Date 3 May 2012.

Ning, J., Liu, J., Kuang, W., Xu, X., Zhang, S., Yan, C., Chi, W., 2018. Spatiotemporal patterns and characteristics of land-use change in China during 2010–2015. J. Geogr. Sci. 28 (5), 547–562. https://doi.org/10.1007/s11442-018-1490-0.

Peng, S., Piao, S., Ciais, P., Friedlingstein, P., Ottle, C., Breon, F.M., Nan, H., Zhou, L., Myneni, R.B., 2012. Surface urban heat island across 419 global big cities. Env. Sci. Technol. 46, 696–703. https://doi.org/10.1021/es2030438.

Perini, K., Magliocco, A., 2014. Effects of vegetation, urban density, building height, and atmospheric conditions on local temperatures and thermal comfort. Urban For. Urban Green. 13, 495–506. https://doi.org/10.1016/j.ufug.2014.03.003.

Shanghai Statistics Bureau, 2015. Shanghai Statistical Yearbook 2014. China Statistics Press, Beijing.

Stocker, T.F., Qin, D., Plattner, G.K., Tignor, M.M.B., Allen, S.K., Boschung, J., Nauels, A., Xia, Y., Bex, V., Midgley, P.M., 2013. Climate change 2013 the physical science basis: Working Group I contribution to the fifth assessment report of the intergovernmental panel on climate change, Climate Change 2013 the Physical Science Basis: Working Group I Contribution to the Fifth Assessment Report of the Intergovernmental Panel on Climate Change. https://doi.org/10.1017/CBO9781107415324.

Tan, J., Zheng, Y., Tang, X., Guo, C., Li, L., Song, G., Zhen, X., Yuan, D., Kalkstein, A.J., Li, F., 2010. The urban heat island and its impact on heat waves and human health in Shanghai. Int. J. Biometeorol. 54, 75–84. https://doi.org/10.1007/s00484-009-0256-x.

Wan Z., Hook S., Hulley G., 2015. MOD11A1 MODIS/Terra Land Surface Temperature/Emissivity Daily L3 Global 1km SIN Grid V006. NASA EOSDIS L. Process. DAAC. https://doi.org/10.5067/MODIS/MOD11A1.006.

Xu, X., 2017. China Population Spatial Distribution Kilometer Grid Dataset. Resource and Environment Data Cloud Platform: Beijing, China. DOI:10.12078/2017121101.

Xu, X., 2017. China GDP Spatial Distribution Kilometer Grid Dataset. Resource and Environment Data Cloud Platform: Beijing, China. DOI:10.12078/2017121102.

Xu, X., Liu, J., Zhang, S., Li, R., Yan, C., Wu, S., 2018. China's Multi-Period Land Use Land Cover Remote Sensing Monitoring Data Set (CNLUCC). Resource and Environment Data Cloud Platform: Beijing, China. DOI:10.12078/2018070201.

Yao, R., Wang, L., Huang, X., Niu, Z., Liu, F., Wang, Q., 2017. Temporal trends of surface urban heat islands and associated determinants in major Chinese cities. Sci. Total Environ. 609, 742–754. https://doi.org/10.1016/j.scitotenv.2017.07.217.

Yao, R., Wang, L., Huang, X., Zhang, W., Li, J., Niu, Z., 2018a. Interannual variations in surface urban heat island intensity and associated drivers in China. J. Env. Manag. 222, 86–94. https://doi.org/10.1016/j.jenvman.2018.05.024.

Yao, R., Wang, L.C., Huang, X., Chen, J.P., Li, J.R., Niu, Z.G., 2018b. Less sensitive of urban surface to climate variability than rural in Northern China. Sci. Total Environ. 628–629, 650–660. https://doi.org/10.1016/j.scitotenv.2018.02.087.

Yao, R., Wang, L., Huang, X., Gong, W., Xia, X., 2019. Greening in rural areas increases the surface urban heat island intensity. Geophys. Res. Lett. 46, 2204–2212. https://doi.org/10.1029/2018GL081816.

Youngsteadt, E., Dale, A.G., Terando, A.J., Dunn, R.R., Frank, S.D., 2015. Do cities simulate climate change? A comparison of herbivore response to urban and global warming. Glob. Chang. Biol. 21, 97–105. https://doi.org/10.1111/gcb.12692.

Zhao, L., Lee, X., Smith, R.B., Oleson, K., 2014. Strong contributions of local background climate to urban heat islands. Nature 511, 216–219. https://doi.org/10.1038/nature13462.

Zhejiang Statistics Bureau, 2015. Zhejiang Statistical Yearbook 2014. China Statistics Press, Beijing.

Zhou, D., Bonafoni, S., Zhang, L., Wang, R., 2018. Remote sensing of the urban heat island effect in a highly populated urban agglomeration area in East China. Sci. Total Environ. 628–629, 415–429. https://doi.org/10.1016/j.scitotenv.2018.02.074.

Zhou, D., Zhang, L., Hao, L., Sun, G., Liu, Y., Zhu, C., 2016. Spatiotemporal trends of urban heat island effect along the urban development intensity gradient in China. Sci. Total Environ. 544, 617–626. https://doi.org/10.1016/j.scitotenv.2015.11.168.

Zhou, D., Zhao, S., Zhang, L., Sun, G., Liu, Y., 2015. The footprint of urban heat island effect in China. Sci. Rep. 5, 11160. https://doi.org/10.1038/srep11160.

Zhou, D.C., Zhao, S.Q., Liu, S.G., Zhang, L.X., Zhu, C., 2014. Surface urban heat island in China's 32 major cities: spatial patterns and drivers. Remote Sens. Environ. 152, 51–61. https://doi.org/10.1016/j.rse.2014.05.017.

Zhou, W.Q., Huang, G.L., Cadenasso, M.L., 2011. Does spatial configuration matter? Understanding the effects of land cover pattern on land surface temperature in urban landscapes. Landsc. Urban Plan. 102, 54–63. https://doi.org/10.1016/j.landurbplan.2011.03.009.

Zhu, X., He, H., Liu, M., Yu, G., Sun, X., Gao, Y., 2010. Spatio-temporal variation of photosynthetically active radiation in China in recent 50 years. J. Geogr. Sci. https://doi.org/10.1007/s11442-010-0812-7.